A versatile fabrication route for screening block copolymer membranes for bioprocessing

Ke Meng,[†] Alberto Alvarez-Fernandez,[‡,¶] Stefan Guldin,[*,‡] and Daniel G. Bracewell[*,†]

[†]*Department of Biochemical Engineering, Gower Street, University College London, London, WC1E 6BT, UK*

[‡]*Department of Chemical Engineering, University College London, Torrington Place, London, WC1E 7HB, UK*

[¶]*Centro de Fisica de Materiales (CFM)(CSICUPV/EHU)-Materials Physics Center (MPC), 20018 San Sebastián, Spain*

E-mail: s.guldin@ucl.ac.uk; d.bracewell@ucl.ac.uk

Abstract

Traditional polyethersulfone (PES) filters, widely used for sterile, viral and ultrafiltration often exhibit limited selectivity-permeability due to the heterogenous pore size distribution. Such limitations have sparked interest in developing novel isoporous membrane materials and fabrication techniques to overcome the selectivity-permeability upper bound. Among several promising candidates, block copolymer membranes produced via the self-assembly and non-solvent induced phase separation (SNIPS) method offer distinct advantages, such as customisable pore size, narrow dispersity, high porosity and mechanical flexibility. However, achieving the desired structure formation in SNIPS remains a complex optimisation procedure, rendering this approach unsuitable for the rapid screening of new block copolymer candidates.

https://doi.org/10.26434/chemrxiv-2024-9vqjf **ORCID:** https://orcid.org/0000-0002-4413-5527 Content not peer-reviewed by ChemRxiv. **License:** CC BY-NC-ND 4.0

This study explores a direct spin coating method to fabricate a poly(styrene)-block-poly(methyl methacrylate) (PS-b-PMMA) thin film composite membrane, integrating a block copolymer layer with rigid anodic aluminium oxide (AAO) support. The process involves depositing the polymer solution onto a water-filled AAO substrate via spin coating. Compared with the SNIPS method, this fabrication process greatly reduces the complexity of optimisation to yield an isoporous membrane structure for filtration purposes. We present this approach as a straightforward and reliable platform method for the rapid screening and evaluation of block copolymer membranes in their initial development stages. When compared to commercial PES membranes with similar molecular weight cut-offs, these novel PS-b-PMMA thin film composite membranes showed similar transmission rates for Bovine Serum Albumin and a Monoclonal Antibody while providing a 9 fold enhancement in Thyroglobulin rejection. This indicates a superior performance in terms of cut-off precision. The membranes demonstrate potential for the removal of viruses and antibody aggregates in the downstream processing of monoclonal antibody production, which could reduce the burden of chromatographic polishing steps. An advance which offers promise for improving efficiency and reducing costs in biopharmaceutical manufacturing.

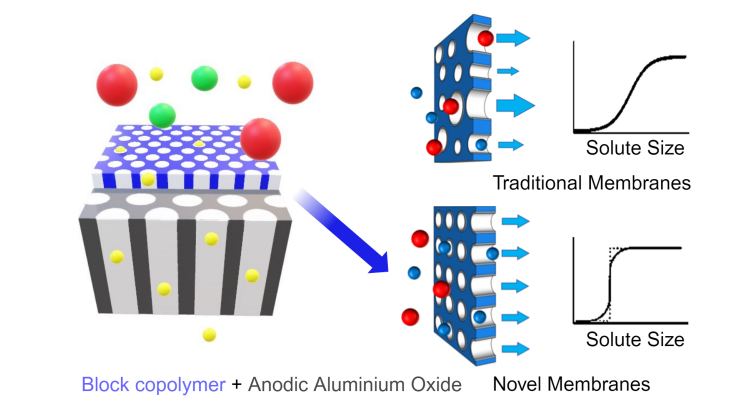

https://doi.org/10.26434/chemrxiv-2024-9vqjf **ORCID:** https://orcid.org/0000-0002-4413-5527 Content not peer-reviewed by ChemRxiv. **License:** CC BY-NC-ND 4.0

INTRODUCTION

Genomic medicines based on viral and non-viral vectors are revolutionising our approach to treating cancer, viral and genetic diseases. However, the intrinsic characteristics of these vectors introduce new challenges for downstream processing associated with their size, stability, and the removal of product-related impurities.[1] Similar challenges are found in antibody manufacture a more established market expected to generate $ 300 billion by 2025[2] with the promise of further growth associated with products for dementia.[3] Critical to all such processes are membrane-based unit operations such as ultrafiltration, virus and sterile filtration, however, many are challenged by low throughput associated with fouling and the demands of meeting the required clearance requirements.[4]

Commercial polyethersulfone (PES) membranes are manufactured using the well-established non-solvent induced phase separation (NIPS) method, pioneered by Loeb and Sourirajan in 1963,[5] and renowned for its versatility and scalability. This characteristic renders them indispensable in various key bio-separation applications for the recovery and purification of monoclonal antibodies, viral vectors, and lipid nanoparticles.[6] Despite their extensive applications, PES membranes still present challenges, particularly regarding their selectivity. This issue, largely attributed to the wide range of pore sizes at the surface separation layer, can significantly impact the efficiency of the filtration process.[7] Such selectivity challenges often lead to product losses or extended processing times, compromising the efficiency of these membranes in practical applications.[8]

Evaluating membrane performance involves a comprehensive analysis based on a series of key parameters, including selectivity, permeability, mechanical integrity, and anti-fouling properties. Each of these parameters is crucial in determining the overall performance of the membrane in special separation challenges.[9] Among them, selectivity and permeability are especially crucial, often exhibiting a "trade-off" relationship in commercial ultrafiltration membranes. Analogous to the renowned Robeson Plot for gas separation membranes,[10,11] this "trade-off" relationship between selectivity and permeability of commercial ultrafiltra-

https://doi.org/10.26434/chemrxiv-2024-9vqjf **ORCID:** https://orcid.org/0000-0002-4413-5527 Content not peer-reviewed by ChemRxiv. **License:** CC BY-NC-ND 4.0

tion membranes was initially investigated by Mehta and Zydney in 2005.[12] The selectivity-permeability data of these commercial NIPS membranes set an "upper bound" and dictated the state-of-the-art performance. This underscores the necessity for innovative materials and fabrication techniques that push beyond the conventional limitations of the selectivity-permeability relationship.[13]

In response to this need, researchers have been investigating a variety of novel materials for developing ultrafiltration membranes with uniform pore size distribution, high porosity, and straight pore channels, as these characteristics are expected to exhibit optimal selectivity-permeability performance[14]. Examples of such materials include self-assembled block copolymer membranes,[15–17] anodic aluminum oxide (AAO) membranes,[18–20] track-etched membranes,[21] microslit silicon nitride (MSN) membranes,[22] and carbon nanotubes.[23] Among these options, block copolymer-based membranes offer unique advantages that have received wide attention. Their formation principles through molecular self-assembly allow the creation of membranes with customisable pore sizes spanning a broad spectrum, narrower pore dispersity, and high porosity.[17] Additionally, their polymeric nature facilitates facile integration into various filtration modules, including the fabrication of hollow fibre membranes.[24,25]

The mechanism for achieving uniform pore formation using block copolymer membranes includes several methods, including self-assembly and non-solvent induced phase separation (SNIPS),[16,26,27] selective etching,[8,9,28] and selective swelling.[29–31] Among these techniques, the SNIPS process demonstrates promising potentials for scale-up,[32,33] as indicated by the emergence of startups like Terapore Tech, which has launched several lab-scale virus filters to the market.[34] However, the SNIPS technique requires the complex integration of block copolymer self-assembly with the NIPS process.[8,35] Careful optimisation of equilibrium and non-equilibrium thermodynamic processes is necessary to achieve a precisely defined membrane with a "honeycomb-like" separation layer and a "sponge-like" supporting structure.[36] While SNIPS is well established for membrane fabrication using well-known block copoly-

https://doi.org/10.26434/chemrxiv-2024-9vqjf **ORCID:** https://orcid.org/0000-0002-4413-5527 Content not peer-reviewed by ChemRxiv. **License:** CC BY-NC-ND 4.0

mer candidates, the complexity of optimisation makes rapid screening of new materials or molecular weight combinations a challenge. Moreover, material demand is significant, since the full membrane architecture is made out of the block copolymers, providing high demands on the synthesis and purification of novel macromolecular candidates.

As an alternative approach, Yang et al.[37] (2005) pioneered the fabrication of block copolymer thin film composite (TFC) membranes via spin coating, annealing, floating, and selective etching, which has demonstrated effectiveness in viral filtration. This technique route generates mesoporous thin film composite membranes with a well-defined separation layer within hundreds of microns.[38] However, this fabrication process remains challenging to achieve in a reliable and reproducible manner. According to our recent experiments, one critical technical challenge is the delamination of the active layer from its support when fabricating PS-b-PMMA thin film composite membranes. Additionally, defects often arise during the floating operation due to the poor mechanical strength of the block copolymer thin film. The application of hydrofluoric acid in this step also introduces safety concerns for the personnel involved. Considering these issues, fabrication methods such as the "salt plate transfer method" and "direct spin-coating" have been proposed and developed.[39–41]

In this work, we employed the direct spin-coating method to deposit PS-b-PMMA thin film onto an AAO microfiltration disc with an average pore size of 0.2 µm as the substrate. AAO discs offer several advantages as substrates: (a) they are hydrophilic, facilitating easy wetting of pores; (b) they have flat and smooth surfaces, which facilitates the coating of a homogeneous thin film; (c) they possess high porosity, making them highly permeable; and (d) they are rigid and incompressible during filtration. To prevent block copolymers from infiltrating the substrate, AAO discs are pre-wetted with Milli-Q water. This allows the formation of a thin active block copolymer with controllable and homogeneous thickness, backed with supportive and permeable substrate. Various feedstocks with a wide range of hydrodynamic sizes were characterised including fluorescein isothiocyanate-dextrans (FITC-dextrans), bovine serum albumin(BSA), monoclonal antibody (mAb), thyroglobulin (Tg),

https://doi.org/10.26434/chemrxiv-2024-9vqjf **ORCID:** https://orcid.org/0000-0002-4413-5527 Content not peer-reviewed by ChemRxiv. **License:** CC BY-NC-ND 4.0

and latex nanoparticles (NPs) to mimic impurities, products and viral particles in the bioseparation processes. This fabrication method could serve as a platform for the rapid screening of block copolymer membrane candidates in early research and development.

MATERIALS AND METHODS

Materials. All chemicals were sourced from common suppliers that are listed below. Block copolymer, poly(styrene)-block-poly(methyl methacrylate) (PS-b-PMMA) with a molecular weight of 180-b-77 kg/mol and a polydispersity index (PDI) of 1.02 was procured from Polymer Source Inc., Canada. Anodisc aluminium oxide membranes, featuring a pore size of 200 nm and a diameter of 25 mm, were sourced from Whatman (catalogue no. 5140520). Biomax polyethersulfone (PES) membranes with molecular weight cut-offs of 50 kDa, 100 kDa, 300 kDa, and 500 kDa, each 25 mm in diameter, were supplied by Millipore, USA. Chemical reagents included glacial acetic acid (catalogue no. 33209) and toluene (catalogue no. 650579), both from Sigma-Aldrich; phosphate buffer saline (PBS) tablets were obtained from Gibco (catalogue no. 18912-014). Milli-Q water was produced using a Milli-Q Academic system by Millipore Merck. Fluorescein isothiocyanate (FITC)-dextran of molecular weights 4 kDa (FD4), 40 kDa (FD40), 150 kDa (46946), and 500 kDa (FD500S) were purchased from Merck Life Science. Nitrogen gas was supplied by BOC. Unmodified polystyrene latex nanoparticles with diameters of 25 nm and 50 nm were acquired from Micromod GmbH, Germany, and those with a diameter of 100 nm were obtained from Merck Life Science (catalogue no. LB1). Thyroglobulin from bovine thyroid and bovine serum albumin were both sourced from Sigma-Aldrich, with catalogue nos. T1001 and A7030, respectively

Fabrication of PS-b-PMMA TFC membranes. The fabrication method used in this work is shown in Figure 1. Firstly, anodisc aluminium oxide microfiltration discs, with a rated pore size of 0.2 µm and a diameter of 25 mm, were wetted in Milli-Q water. They were then placed on a 3 cm × 3 cm square plasma-cleaned silicon wafer. Before the block

https://doi.org/10.26434/chemrxiv-2024-9vqjf **ORCID:** https://orcid.org/0000-0002-4413-5527 Content not peer-reviewed by ChemRxiv. **License:** CC BY-NC-ND 4.0

copolymer solution was coated, a spinning test was performed to assess the adhesion between the AAO and the silicon substrate. The AAO disc should be firmly attached to the silicon wafer surface at rotational speeds of up to 5000 rpm. The adhesion was due to the water filling the interspace between the two materials. Wetting the AAO samples also prevented the PS-b-PMMA solution from penetrating the pores during the spin-coating step, as PS-b-PMMA and toluene are immiscible with water.

Subsequently, a 4 wt. % PS-b-PMMA solution dissolved in toluene was prepared and filtered through a 0.45 µm PTEF syringe filter to remove any possible dust. The polymeric solution was then spread over the entire surface of the AAO disc, and spinning was initiated at 1000 rpm for 60 seconds. Once the spin-coating was completed, the membrane sample was carefully detached from the silicon wafer substrate using tweezers, holding it at the plastic O-ring area due to the brittleness of the AAO discs. The membrane sample was then transferred to an Amicon stirred cell for acetic acid etching until a steady flux was observed. Afterwards, the sample was flushed with Milli-Q water and left to dry at room temperature overnight, for subsequent SEM and AFM characterisation.

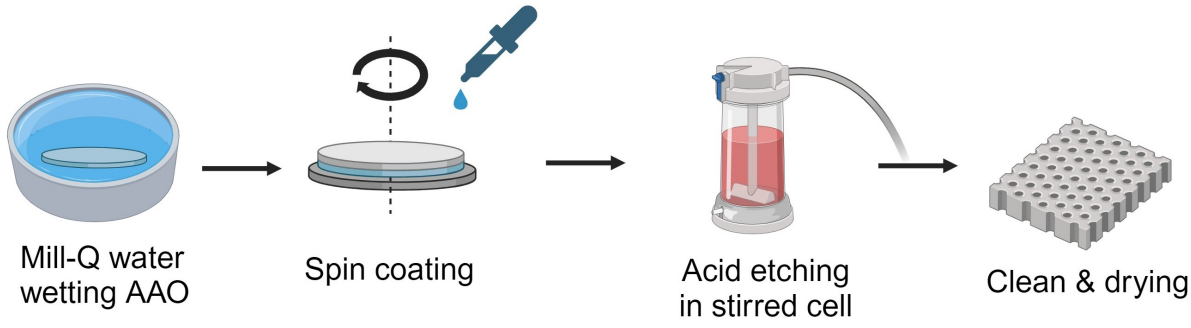

Figure 1: A schematic diagram of the fabrication of block copolymer membrane used in this work.[42]

Surface characterisation of PS-b-PMMA TFC membranes. Atomic Force Microscopy (AFM) was performed using a Bruker Dimension Icon with post-processing and image analysis via NanoScope Analysis 1.5 and WSxM 5.0.[43] The AFM probes were obtained from ScanAsyst-Air from Bruker. For SEM, a sputter coater, Quorum SC7620, was

https://doi.org/10.26434/chemrxiv-2024-9vqjf ORCID: https://orcid.org/0000-0002-4413-5527 Content not peer-reviewed by ChemRxiv. License: CC BY-NC-ND 4.0

used to deposit a thin layer of gold to improve imaging quality. The SEM imaging was carried out with a Carl Zeiss XB1540 Cross-Beam system from Germany. The instrument operated at a voltage of 10 kV, utilising an SE2 signal source, and achieved imaging magnifications ranging from 13,000x to 16,000x.

Ultrafiltration. The experimental setups for the selectivity and permeability tests are illustrated in Figure S3 (Supporting Information). Membrane candidates in 25 mm diameter were loaded into the Amicon stirred cell (model 8010), sourced from Merck Millipore. Various detectors such as Thermo Fisher Uv-vis Spectrometer G10S, Shimadzu refractive index detector, and Shimadzu RF-6000 spectro-fluorophotometer were used to measure the concentration of feed and permeate.

Size exclusion chromatography (SEC). A Shimadzu 2030 HPLC system, along with a TSKgel G5000PWXL (08023) size exclusion chromatography column from Tosoh, was used to fractionate dextran of different molecular weights. A refractive index detector (RID-20A from Shimadzu) was used to detect the concentration of dextran. The column was calibrated with monodisperse dextran standards (Sigma Aldrich) of varying molecular weights to correlate retention time with molecular weight. The mobile phase was 1 × PBS buffer running at 0.3 ml/min due to the pressure restrictions of the size exclusion column.

RESULTS AND DISCUSSION

Characterisation of PS-b-PMMA TFC membranes

The spin coating requires a flat and rigid surface as the support structure for holding the membrane backing material and coating the polymeric solution. As is shown in Figure 2 (a), this was achieved by depositing the fully wetted AAO microfiltration disc onto the plasma-cleaned silicon wafer. To fabricate the composite membranes, the PS-b-PMMA thin film was spin-coated on the AAO disc and etched with acetic acid. It appeared uniformly transparent after being wetted by Milli-Q water, as shown in Figure 2 (b).

https://doi.org/10.26434/chemrxiv-2024-9vqjf **ORCID:** https://orcid.org/0000-0002-4413-5527 Content not peer-reviewed by ChemRxiv. **License:** CC BY-NC-ND 4.0

The sample was then cut in the middle for top surface and cross-sectional imaging by SEM. As depicted in Figure 2 (c), the top view image shows the thin PS-b-PMMA layer as a homogeneous selective layer and the long AAO channels as the backing layer. The edge of the PS-b-PMMA thin film appeared partially lifted as a consequence of the mechanical cutting. At the interface, there was no evidence of blockage to the AAO backing layer by PS-b-PMMA, as intended with this novel fabrication design. In addition, there were no delamination or defect issues for this direct spin coating method, unlike those previously attempted using the floating technique, as shown in Figure S1 (Supporting Information). A cross-sectional SEM image of the bottom side of the AAO substrate shows the expected long and straight pore channels of approximately 0.2 µm in size, see Figure 2 (d).

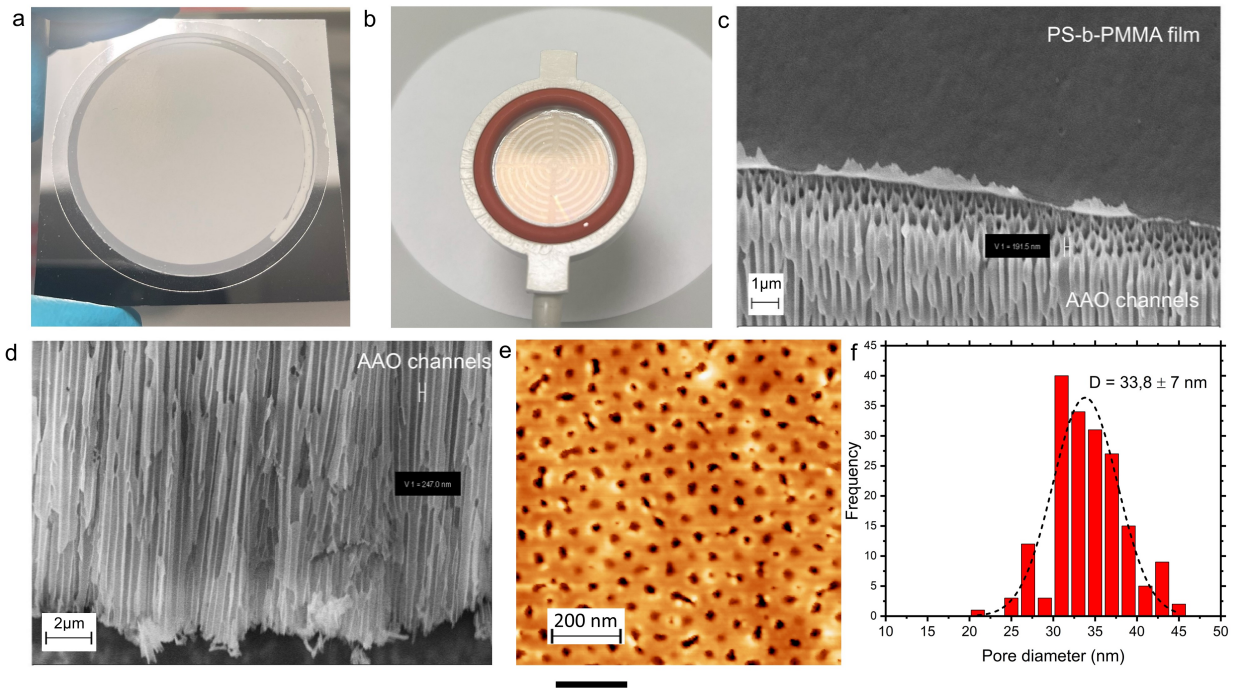

Figure 2: (a) Photograph of a water-wetted anodisc aluminium oxide (AAO) disc settled on a silicon wafer, (b) Photograph of a PS-b-PMMA thin film coated on AAO composite membrane after the etching step that is fixed in the O-ring of the stirred cell, (c) SEM image of the cross-sectional area of an etched PS-b-PMMA TFC membrane, (d) SEM image of the bottom side of the TFC membrane that are aluminium oxide channels, (e) AFM image of PS-b-PMMA TFC membrane at the membrane surface after water flux filtration with pore size identification of the sample by software Pebble, (f) Pore size distribution analyse of the sample by PebbleJuggler.[44]

https://doi.org/10.26434/chemrxiv-2024-9vqjf ORCID: https://orcid.org/0000-0002-4413-5527 Content not peer-reviewed by ChemRxiv. License: CC BY-NC-ND 4.0

AFM imaging was used to investigate the self-assembled morphology of the block copolymer selective layer and to demonstrate the impact of acid etching. After acid etching, the membrane sample was flushed with water at 1 bar for approximately 30 minutes to remove any residual acid, and then properly dried at room temperature. It was attached to a silicon wafer substrate to secure it to the AFM specimen support. As shown in Figure 2(e), the PMMA block in the selective layer was removed by acetic acid, resulting in self-assembled pore morphology. However, the structural order becomes more dispersed when compared to the PS-b-PMMA thin film directly spin-coated on the silicon wafer, see Figure S2 (Supporting Information). The average pore size diameter was 33.8 nm ± 7 nm. A few tiny pores (less than 5 nm) were also scattered across the membrane surface, which could be attributed to the less-ordered block copolymers at the surface.

Characterisation on Feedstocks

Proteins and latex nanoparticles

Unmodified spherical and monodisperse fluorescence latex nanoparticles have been used to validate the performance of sterile filters by mimicking the physical properties of viral products in recent years.[45,46] Their excitation wavelength is typically 552 nm, and emission wavelength 580 nm. As illustrated in Figure 3(a) and (b), the 25 nm and 50 nm latex NPs were formulated at 10 g/L and showed a light pink colour. These were further diluted to concentrations between 0.1 g/L and 0.01 g/L for spectro-fluorophotometer measurements because a higher concentration of the sample exceeded the upper bound of the detection range. Three protein feedstocks of BSA, mAb and thyroglobulin (Tg) were prepared at 1 g/L in PBS buffer. The standard curve for all three proteins exhibited a strong linear correlation at 280 nm ($R^2 = 0.99$), see Figure 3 (c).

https://doi.org/10.26434/chemrxiv-2024-9vqjf **ORCID:** https://orcid.org/0000-0002-4413-5527 Content not peer-reviewed by ChemRxiv. **License:** CC BY-NC-ND 4.0

FITC-dextrans

Shown in Figure 3 (d), Fluorescein isothiocyanate (FITC)-dextrans are dextran particles linked with fluorescent labels and were used to study membrane permeability.[47] Molecular weights (MWs) of 4 kDa, 40 kDa, 150 kDa, and 500 kDa were used to mimic the sizes of organic acids, abundant host cell proteins, mAb, and mAb aggregates, respectively, as feedstocks for investigating the selectivity performance of the membrane candidates.[48,49]

As is shown in Figure 3 (e), FITC dextran samples with larger average molecular weight are more dispersed according to the SEC chromatogram. Among them, the 150 kDa FITC-dextran has a wider size distribution than other molecules. The overlapped negative peaks in all samples at about 36 minutes are likely due to additives or small sugar molecules in the dextran samples, such as glucose.

Since FITC dextran is not UV/vis sensitive, the intensity of FITC-dextran was measured using a spectro-fluorophotometer from Shimadzu. Figure 3(f) shows that the relationship between signal intensity and concentration follows a strong linear relationship with R2 = 0.999. However, the detectable concentration of FITC-dextran ranges from 0.001 mg/ml to 0.01 mg/ml. Higher concentrations of FITC-dextran emit stronger signals that exceed the upper limit of the spectro-fluorophotometer. Therefore, 0.01 mg/ml of FITC-dextrans were prepared separately and used for challenging membrane candidates.

https://doi.org/10.26434/chemrxiv-2024-9vqjf **ORCID:** https://orcid.org/0000-0002-4413-5527 Content not peer-reviewed by ChemRxiv. **License:** CC BY-NC-ND 4.0

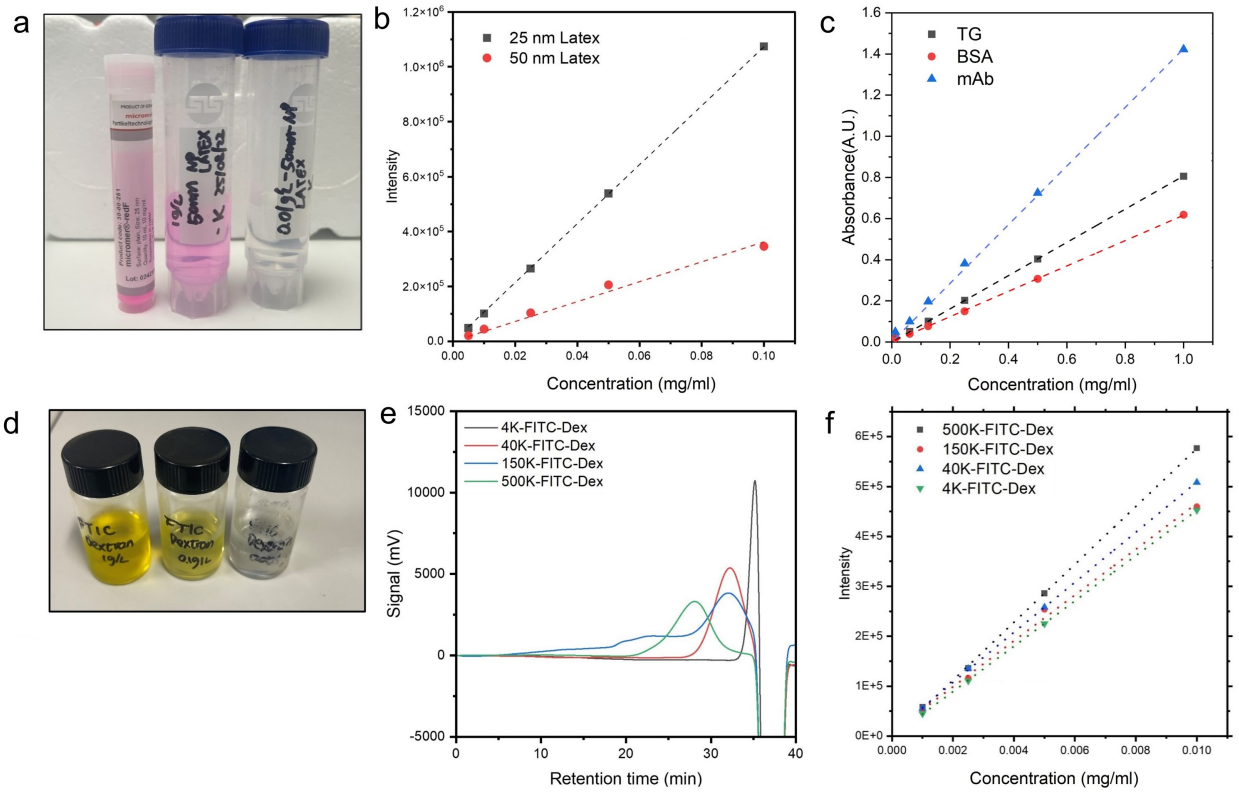

Figure 3: (a) 50 nm latex NP solution at 10 g/L, 1 g/L and 0.01 g/L, (b) Calibration curve of the intensity of fluorescence of 25 nm and 50 nm latex NP at different concentrations by spectro-fluorophotometer (R^2=0.99), (c) The standard curve for bovine serum albumin (BSA), Trastuzumab(mAb) and thyroglobulin (Tg) measurement at optical absorption 280 nm at pH 7.0, measured by a spectrofluorophotometer (R^2=0.99), (d) 500 kDa FITC-dextran solution at 1 g/L, 0.1 g/L and 0.01 g/L, (e) Characterisation of FITC-dextran with MW 4 kDa, 40 kDa, 150 kDa, and 500 kDa by size exclusion chromatography, (f) The calibration curve of the intensity of fluorescent FITC-Dextran 4 kDa, 40 kDa, 150 kDa, 500 kDa at different concentration (R^2=0.99).

https://doi.org/10.26434/chemrxiv-2024-9vqjf **ORCID:** https://orcid.org/0000-0002-4413-5527 Content not peer-reviewed by ChemRxiv. **License:** CC BY-NC-ND 4.0

Filtration experiments

The permeability and selectivity of PS-b-PMMA TFC membranes were examined in the Amicon stirred cell, where the set-up is illustrated in Figure S3 (Supporting Information). Water permeability tests were performed to benchmark the candidate with commercially available PES ultrafiltration membranes. The selectivity performance of PS-b-PMMA was compared with 100, 300, and 500 kDa PES membranes as positive controls and AAO 0.2 μm discs as negative controls, each with three replicates. All filtration measurements were conducted in the Amicon stirred cell 8010 at 0.6 bar and 600 rpm.

FITC-Dextrans rejection

The concentration of FITC-dextrans as feedstock and permeate was measured by a spectro-fluorophotometer. As is shown in Figure 4 (a), a double plot includes a bar chart in blue that represents the rejection rate and the dotted curves in black and red that indicate the normalised intensity of permeate (filtrate) of FITC-dextrans by passing through a PS-b-PMMA TFC membrane and an AAO disc (backing material alone) as the control group. The PS-b-PMMA TFC membrane achieved more than 60% rejection at 500 kDa, allowing most lower molecular weight dextran at 4 kDa and 40 kDa to pass through. This indicates that the membrane candidate exhibits size-based selectivity. The dotted curve in red represents the ratio of fluorescence signal in the permeate to the feedstock, also known as the sieving coefficient. The sieving coefficient of dextrans at 4 kDa and 40 kDa is approaching 1, which means minimal adsorption of dextrans at the surface of the membrane candidates. The black curve represents the control group of AAO backing materials contributing a minimal amount of rejection of FITC-dextrans across all molecular weights from 4 kDa to 500 kDa. However, the molecular weight of FITC-dextrans cannot cover the molecular weight cut-off (MWCO) of the membrane candidate, defined as the 90% of the feed being rejected. Therefore, further sieving experiments involving proteins and latex NPs were conducted to screen the membrane candidates' selectivity.

https://doi.org/10.26434/chemrxiv-2024-9vqjf **ORCID:** https://orcid.org/0000-0002-4413-5527 Content not peer-reviewed by ChemRxiv. **License:** CC BY-NC-ND 4.0

Water permeability

As shown in Figure 4 (b), water permeability data for a series of Biomax commercial PES membranes and PS-b-PMMA TFC membranes with 3 replicates each, were measured. For all candidate membranes, the relationship between the water flux (LMH) and transmembrane pressures (bars) demonstrates a strong linear fit ($R^2 = 0.99$). The water permeability of the PS-b-PMMA TFC membrane (154 ± 9.2 LMH/bars) is less than half of that of the 50 kDa PES (383 ± 9.68 LMH/bars) membranes, which could be further improved. This could be done by reducing the thickness of the selective layer in the spin-coating step or improving the ordering of block copolymer self-assembly by annealing steps for forming straighter pore channels.

Proteins and latex NPs Rejection

The selectivity performance of PS-b-PMMA TFC was assessed against PES membranes of 100 kDa, 300 kDa, and 500 kDa, serving as positive controls. Additionally, AAO 0.2 μm discs were used as negative controls, each with three replicates. As illustrated in Figure 4(c), the rejection profile of the AAO discs (shown in blue) in the negative control group showed a gradual increase, ranging from 10% in filtering BSA, mAb, and Tg, to over 90% in filtering 50 nm latex NPs.

In contrast, the rejection profile of the PS-b-PMMA TFC membranes (shown in red) was markedly sharper, showing over 90% rejection of Tg and latex NPs, but retaining less than 10% retention for mAb and BSA. Notably, the PS-b-PMMA TFC membrane exhibited more than 95% rejection of 25 nm latex NPs and over 99% 50 nm latex NPs, despite the observed surface average pore size of the membrane being approximately 38 nm.

Among commercial PES membranes (Figure 4d), the 300 kDa and 500 kDa membranes showed similar rejection profiles. Over 90% of BSA, mAb, and Tg infiltrated through both membranes, while over 95% of 25 nm and 50 nm latex NPs were rejected. The 100 kDa PES membranes also showed over 90% rejection of all three proteins and latex NPs, exhibiting a

https://doi.org/10.26434/chemrxiv-2024-9vqjf **ORCID:** https://orcid.org/0000-0002-4413-5527 Content not peer-reviewed by ChemRxiv. **License:** CC BY-NC-ND 4.0

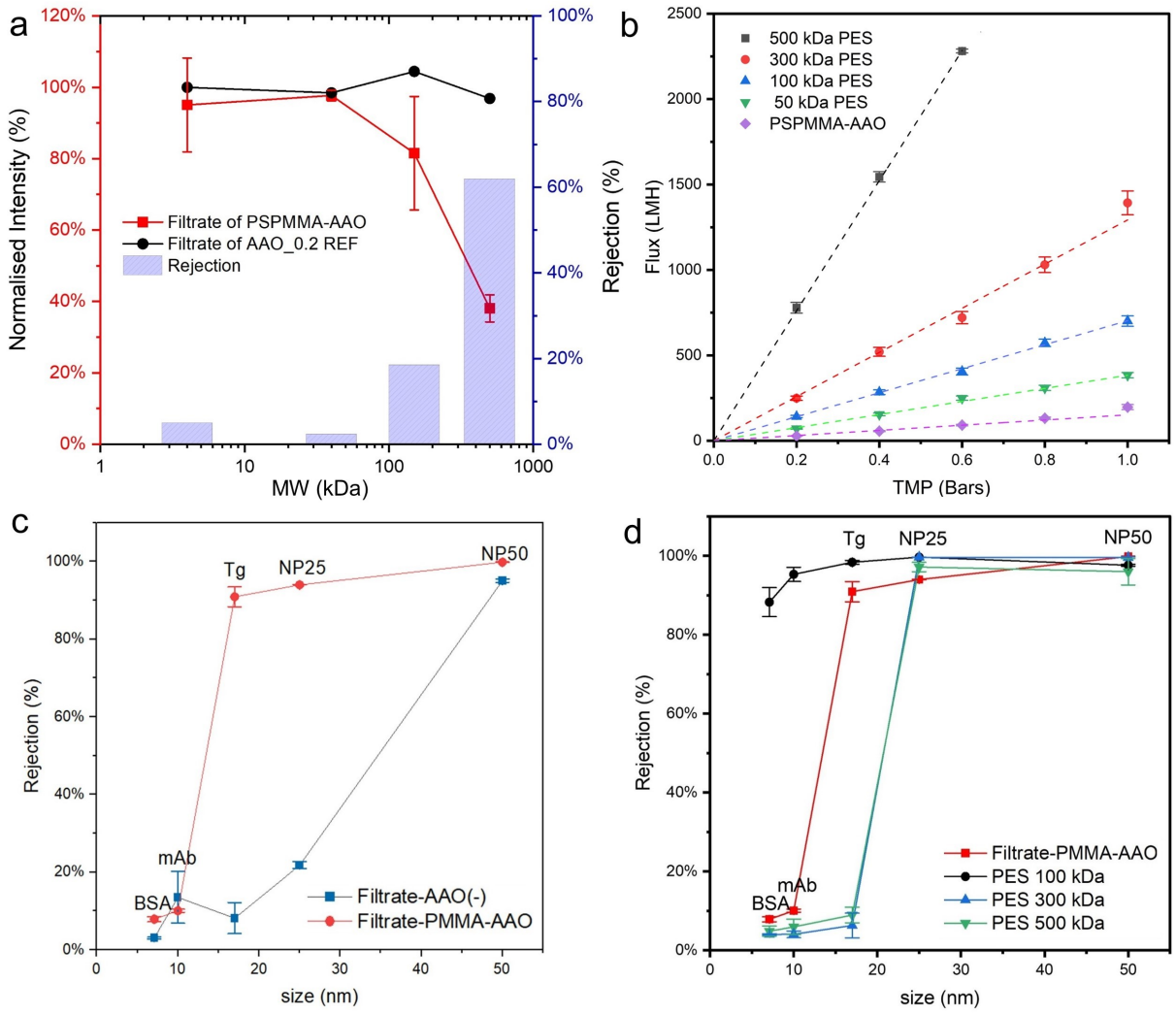

Figure 4: (a) The rejection rate of FITC-Dextrans at different molecular weights for PS-b-PMMA TFC membrane (red) and AAO disc alone (black), (b) The permeability performance of a well etched PS-b-PMMA TFC membrane (R^2=0.99), benchmarked with commercial 50 kDa, 100 kDa, 300 kDa and 500 kDa PES membranes, (c) Rejection rate of a PS-b-PMMA TFC membrane, tested by BSA, mAb (trastuzumab), Tg (Thyroglobulin), and latex NP 25 nm and 50 nm, benchmarked with microfiltration AAO disc with pore size 200 nm, (d) The same rejection rate of a PS-b-PMMA TFC membrane, compared with commercial PES 100, 300, 500 kDa membranes.

https://doi.org/10.26434/chemrxiv-2024-9vqjf **ORCID:** https://orcid.org/0000-0002-4413-5527 Content not peer-reviewed by ChemRxiv. **License:** CC BY-NC-ND 4.0

broader rejection spectrum.

An interesting observation is that the PS-b-PMMA TFC membranes can effectively differentiate between monoclonal antibodies (mAbs) and thyroglobulin (Tg) based on molecular weight. In contrast, the chosen commercial polyethersulfone (PES) membranes failed to separate proteins of different sizes, possibly due to a wider distribution of surface pore sizes. Moreover, it also indicates that the molecular weight cut-off (MWCO) of the PS-b-PMMA TFC membrane ranges between 100 kDa and 300 kDa.

From an application standpoint, the rejection data indicate that the 300 kDa and 500 kDa PES membranes can be used to separate antibodies from larger viruses with diameters above 25 nm. In comparison, the PS-b-PMMA TFC membrane could remove smaller viruses, such as the Minute Virus of Mice (MVM), and even antibody aggregates from the feedstock. This filtration as a unit operation could potentially reduce downstream processing burdens, such as the need for chromatography polishing steps.

Post-filtration SEM imaging

SEM was conducted on PS-b-PMMA TFC membranes that were filtered with 100 nm latex NP, as nanoparticles at the size could be visualised. The post-filtration imaging aims to demonstrate that the membrane candidate has successfully retained the experimented feedstock. As depicted in Figure 5, the latex NPs have accumulated to form a dense cake layer on the membrane's top surface, while the AAO channels remain free of latex nanoparticles. This demonstrates that the PS-b-PMMA TFC membrane can effectively reject latex nanoparticles, which matches with experimental filtration results. This suggests its potential applications for large virus retention or removal.

https://doi.org/10.26434/chemrxiv-2024-9vqjf **ORCID:** https://orcid.org/0000-0002-4413-5527 Content not peer-reviewed by ChemRxiv. **License:** CC BY-NC-ND 4.0

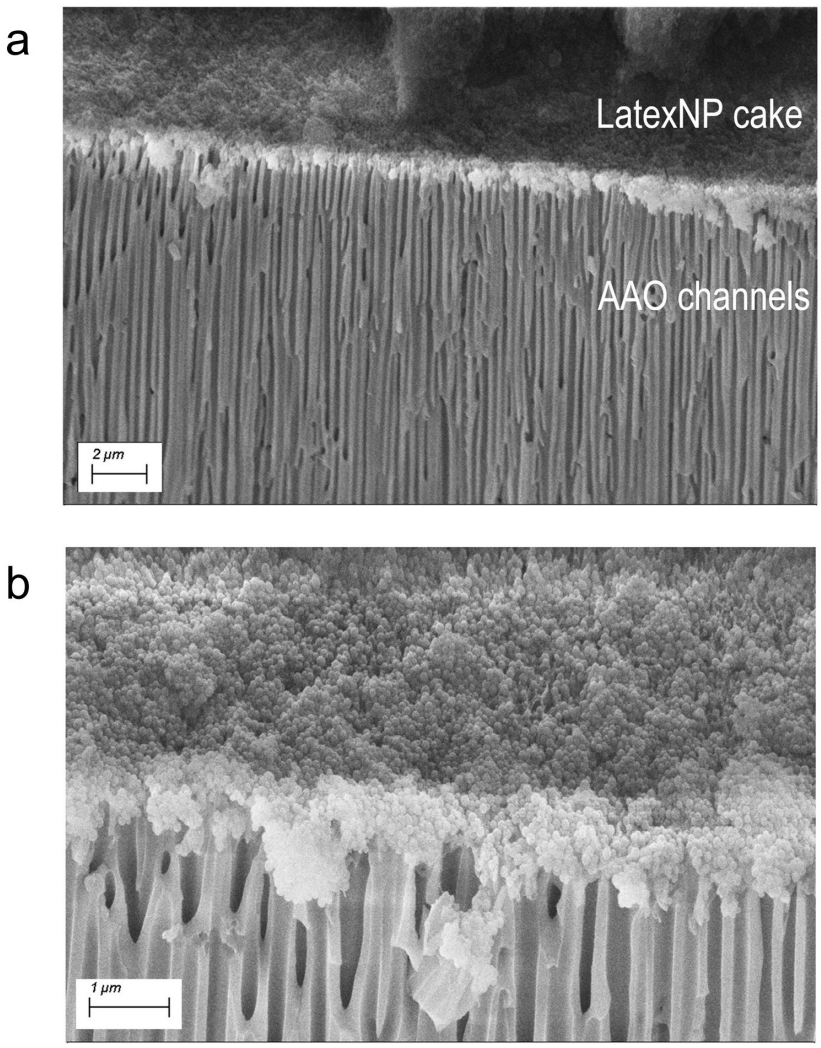

Figure 5: SEM imaging of a PS-b-PMMA TFC membrane after filtered with 100 nm latex NP at different locations.

https://doi.org/10.26434/chemrxiv-2024-9vqjf **ORCID:** https://orcid.org/0000-0002-4413-5527 Content not peer-reviewed by ChemRxiv. **License:** CC BY-NC-ND 4.0

Conclusions

This study presents a novel fabrication methodology for PS-b-PMMA TFC membranes by direct spin-coating onto AAO discs, followed by selective acid etching in the stirred cell device. The surface characteristics under AFM and SEM appeared promising with no potential defects, pore blockages or delamination issues, and surface pores were properly etched. Selectivity results indicate that PS-b-PMMA TFC membranes reject over 90% of Tg and latex NPs, but less than 10% of mAb and BSA. Compared to commercial PES membranes, the MWCO of PS-b-PMMA TFC membrane falls within the range's characteristic of 100 kDa and 300 kDa membranes. The rejection profile of the candidate suggests that its selectivity performance is comparable to that of the commercial 300 kDa and 500 kDa PES membranes.

The work established a facile fabrication method for a PS-b-PMMA thin film composite membrane containing a thin layer of block copolymer and a rigid AAO as the backing support. Compared with the SNIPS method, this is greatly simplified and requires less complex optimisation procedures, creating an isoporous membrane structure for filtration purposes. We believe that this method presents a useful and effective platform for rapidly screening block copolymer membranes in the early development stages. From an application standpoint, given the physical similarity between Tg and small viruses,[20] this membrane candidate shows potential for use in removing parvoviruses during the downstream processing in monoclonal antibody production. Future work could focus on improving the permeability performance of membranes by enhancing the ordering of pore channels or reducing the thickness of selective layers in the fabrication stages, such as different annealing strategies.

https://doi.org/10.26434/chemrxiv-2024-9vqjf **ORCID:** https://orcid.org/0000-0002-4413-5527 Content not peer-reviewed by ChemRxiv. **License:** CC BY-NC-ND 4.0

Acknowledgements

KM acknowledges the Engineering and Physical Sciences Research Council (EPSRC) for funding via EPSRC-SFI the Centre for Doctoral Training in Advanced Characterisation of Materials, grant EP/S023259/1. He is also grateful to UCL Department of Biochemical Engineering and Chemical Engineering for financial and facility support of his PhD study.

Supporting Information Available

The Supporting Information is available in the following pages:

https://doi.org/10.26434/chemrxiv-2024-9vqjf **ORCID:** https://orcid.org/0000-0002-4413-5527 Content not peer-reviewed by ChemRxiv. **License:** CC BY-NC-ND 4.0

References

(1) Segura, M. M.; Kamen, A. A.; Garnier, A. Overview of current scalable methods for purification of viral vectors. 2011.

(2) Lu, R. M.; Hwang, Y. C.; Liu, I. J.; Lee, C. C.; Tsai, H. Z.; Li, H. J.; Wu, H. C. Development of therapeutic antibodies for the treatment of diseases. *Journal of Biomedical Science* **2020**, *27*.

(3) Rahman, A.; Hossen, M. A.; Chowdhury, M. F. I.; Bari, S.; Tamanna, N.; Sultana, S. S.; Haque, S. N.; Masud, A. A.; Saif-Ur-Rahman, K. M. Aducanumab for the treatment of Alzheimer's disease: a systematic review. *Psychogeriatrics* **2023**, *23*.

(4) Isu, S.; Qian, X.; Zydney, A. L.; Wickramasinghe, S. R. Process-and Product-Related Foulants in Virus Filtration. *Bioengineering* **2022**, *9*.

(5) Loeb, S.; Sourirajan, S. Sea Water Demineralization by Means of an Osmotic Membrane. In Saline Water Conversion-II Chapter 9. *Advances in Chemistry, ACS* **1963**, *38*, 117–132.

(6) Lv, J.; Muhammad, N.; Lan, J.; Song, H. Pore structure regulation and continuous preparation with VNIPS process of membranes for bioseparation. *Separation and Purification Technology* **2024**, *334*, 125936.

(7) Zhang, Y.; Almodovar-Arbelo, N. E.; Weidman, J. L.; Corti, D. S.; Boudouris, B. W.; Phillip, W. A. Fit-for-purpose block polymer membranes molecularly engineered for water treatment. *npj Clean Water* **2018**, *1*, 1–14.

(8) Hampu, N.; Werber, J. R.; Chan, W. Y.; Feinberg, E. C.; Hillmyer, M. A. Next-Generation Ultrafiltration Membranes Enabled by Block Polymers. *ACS Nano* **2020**, *14*, 16446–16471.

https://doi.org/10.26434/chemrxiv-2024-9vqjf **ORCID:** https://orcid.org/0000-0002-4413-5527 Content not peer-reviewed by ChemRxiv. **License:** CC BY-NC-ND 4.0

(9) Phillip, W. A.; Hillmyer, M. A.; Cussler, E. L. Cylinder orientation mechanism in block copolymer thin films upon solvent evaporation. *Macromolecules* **2010**, *43*, 7763–7770.

(10) Robeson, L. M. Correlation of separation factor versus permeability for polymeric membranes. *Journal of Membrane Science* **1991**, *62*, 165–185.

(11) Robeson, L. M. The upper bound revisited. *Journal of Membrane Science* **2008**, *320*, 390–400.

(12) Mehta, A.; Zydney, A. L. Permeability and selectivity analysis for ultrafiltration membranes. *Journal of Membrane Science* **2005**, *249*, 245–249.

(13) Park, H. B.; Kamcev, J.; Robeson, L. M.; Elimelech, M.; Freeman, B. D. Maximizing the right stuff: The trade-off between membrane permeability and selectivity. *Science* **2017**, *356*, 1138–1148.

(14) Waldman, R. Z.; Gao, F.; Phillip, W. A.; Darling, S. B. Maximizing selectivity: An analysis of isoporous membranes. *Journal of Membrane Science* **2021**, *633*, 119389.

(15) Peinemann, K. V.; Abetz, V.; Simon, P. F. Asymmetric superstructure formed in a block copolymer via phase separation. *Nature Materials* **2007**, *6*, 992–996.

(16) Dorin, R. M.; Sai, H.; Wiesner, U. Hierarchically porous materials from block copolymers. *Chemistry of Materials* **2014**, *26*, 339–347.

(17) Nunes, S. P. *Sustainable Nanoscale Engineering From Materials Design to Chemical Processing*; Elsevier Inc., 2020; Chapter 11, pp 297–316.

(18) Osmanbeyoglu, H. U.; Hur, T. B.; Kim, H. K. Thin alumina nanoporous membranes for similar size biomolecule separation. *Journal of Membrane Science* **2009**, *343*, 1–6.

(19) Jeon, G.; Jee, M.; Yang, S. Y.; Lee, B. Y.; Jang, S. K.; Kim, J. K. Hierarchically self-organized monolithic nanoporous membrane for excellent virus enrichment. *ACS Applied Materials and Interfaces* **2014**, *6*, 1200–1206.

https://doi.org/10.26434/chemrxiv-2024-9vqjf **ORCID:** https://orcid.org/0000-0002-4413-5527 Content not peer-reviewed by ChemRxiv. **License:** CC BY-NC-ND 4.0

(20) Sharma, A.; Bracewell, D. G. Characterisation of porous anodic alumina membranes for ultrafiltration of protein nanoparticles as a size mimic of virus particles. *Journal of Membrane Science* **2019**, *580*, 77–91.

(21) Sabirova, A.; Pisig, F.; Rayapuram, N.; Hirt, H.; Nunes, S. P. Nanofabrication of Isoporous Membranes for Cell Fractionation. *Scientific Reports* **2020**, *10*, 1–9.

(22) Wright, E.; Miller, J. J.; Csordas, M.; Gosselin, A. R.; Carter, J. A.; McGrath, J. L.; Latulippe, D. R.; Roussie, J. A. Development of isoporous microslit silicon nitride membranes for sterile filtration applications. *Biotechnology and Bioengineering* **2019**, 1–7.

(23) Holt, J. K.; Park, H. G.; Wang, Y.; Stadermann, M.; Artyukhin, A. B.; Grigoropoulos, C. P.; Noy, A.; Bakajin, O. Fast mass transport through sub-2-nanometer carbon nanotubes. *Science* **2006**, *312*, 1034–1038.

(24) Nunes, S. P.; Behzad, A. R.; Peinemann, K.-V. Self-assembled block copolymer membranes: From basic research to large-scale manufacturing. *Journal of Materials Research* **2013**, *28*, 2661–2665.

(25) Radjabian, M.; Koll, J.; Buhr, K.; Handge, U. A.; Abetz, V. Hollow fiber spinning of block copolymers: Influence of spinning conditions on morphological properties. *Polymer* **2013**, *54*, 1803–1812.

(26) Karunakaran, M.; Nunes, S. P.; Qiu, X.; Yu, H.; Peinemann, K. V. Isoporous PS-b-PEO ultrafiltration membranes via self-assembly and water-induced phase separation. *Journal of Membrane Science* **2014**, *453*.

(27) Shevate, R.; Kumar, M.; Cheng, H.; Hong, P. Y.; Behzad, A. R.; Anjum, D.; Peinemann, K. V. Rapid Size-Based Protein Discrimination inside Hybrid Isoporous Membranes. *ACS Applied Materials and Interfaces* **2019**, *11*, 8507–8516.

https://doi.org/10.26434/chemrxiv-2024-9vqjf **ORCID:** https://orcid.org/0000-0002-4413-5527 Content not peer-reviewed by ChemRxiv. **License:** CC BY-NC-ND 4.0

(28) Zhou, H. J.; Yang, G. W.; Zhang, Y. Y.; Xu, Z. K.; Wu, G. P. Bioinspired Block Copolymer for Mineralized Nanoporous Membrane. *ACS Nano* **2018**, *12*, 11471–11480.

(29) Ahn, H.; Park, S.; Kim, S. W.; Yoo, P. J.; Ryu, D. Y.; Russell, T. P. Nanoporous block copolymer membranes for ultrafiltration: A simple approach to size tunability. *ACS Nano* **2014**, *8*.

(30) Yao, X.; Guo, L.; Chen, X.; Huang, J.; Steinhart, M.; Wang, Y. Filtration-based synthesis of micelle-derived composite membranes for high-flux ultrafiltration. *ACS Applied Materials and Interfaces* **2015**, *7*.

(31) Guo, L.; Wang, L.; Wang, Y. Stretched homoporous composite membranes with elliptic nanopores for external-energy-free ultrafiltration. *Chemical Communications* **2016**, *52*.

(32) Nunes, S. P. Block Copolymer Membranes for Aqueous Solution Applications. *Macromolecules* **2016**, *49*, 2905–2916.

(33) Nunes, S. P.; Culfaz-Emecen, P. Z.; Ramon, G. Z.; Visser, T.; Koops, G. H.; Jin, W.; Ulbricht, M. Thinking the future of membranes: Perspectives for advanced and new membrane materials and manufacturing processes. *Journal of Membrane Science* **2020**, *598*, 117761.

(34) Teraporetech Inc. `Teraporetech.com`, 2024; [Online; accessed 15-February-2024].

(35) Hamta, A.; Ashtiani, F. Z.; Karimi, M.; Moayedfard, S. Asymmetric block copolymer membrane fabrication mechanism through self-assembly and non-solvent induced phase separation (SNIPS) process. *Scientific Reports* **2022**, *12*.

(36) Radjabian, M.; Abetz, V. Advanced porous polymer membranes from self-assembling block copolymers. *Progress in Polymer Science* **2020**, 101219.

(37) Yang, S.; Ryu, I.; Kim, H. Y.; Kim, J. K.; Jang, S. K.; Russell, T. P. Nanoporous

https://doi.org/10.26434/chemrxiv-2024-9vqjf **ORCID:** https://orcid.org/0000-0002-4413-5527 Content not peer-reviewed by ChemRxiv. **License:** CC BY-NC-ND 4.0

membranes with ultrahigh selectivity and flux for the filtration of viruses. *Advanced Materials* **2006**, *18*, 709–712.

(38) Yang, S.; Park, J.; Yoon, J.; Ree, M.; Jang, S. K.; Kim, J. K. Virus filtration membranes prepared from nanoporous block copolymers with good dimensional stability under high pressures and excellent solvent resistance. *Advanced Functional Materials* **2008**, *18*, 1371–1377.

(39) Li, F.; Vijayasankaran, N.; Shen, A.; Kiss, R.; Amanullah, A. Cell culture processes for monoclonal antibody production. *mAbs* **2010**, *2*, 466–479.

(40) Jackson, E. A.; Lee, Y.; Hillmyer, M. A. ABAC tetrablock terpolymers for tough nanoporous filtration membranes. *Macromolecules* **2013**, *46*, 1484–1491.

(41) Querelle, S. E.; Jackson, E. A.; Cussler, E. L.; Hillmyer, M. A. Ultrafiltration membranes with a thin poly(styrene)- b -poly(isoprene) selective layer. *ACS Applied Materials and Interfaces* **2013**, *5*, 5044–5050.

(42) Aoki, S. BIORENDER. *Biorender* **2017**,

(43) Horcas, I.; Fernández, R.; Gómez-Rodríguez, J. M.; Colchero, J.; Gómez-Herrero, J.; Baro, A. M. WSXM: A software for scanning probe microscopy and a tool for nanotechnology. *Review of Scientific Instruments* **2007**, *78*.

(44) Mondini, S.; Ferretti, A. M.; Puglisi, A.; Ponti, A. Pebbles and PebbleJuggler: Software for accurate, unbiased, and fast measurement and analysis of nanoparticle morphology from transmission electron microscopy (TEM) micrographs. *Nanoscale* **2012**, *4*.

(45) Taylor, N.; Ma, W.; Kristopeit, A.; Wang, S. C.; Zydney, A. L. Evaluation of a sterile filtration process for viral vaccines using a model nanoparticle suspension. *Biotechnology and Bioengineering* **2021**, *118*.

https://doi.org/10.26434/chemrxiv-2024-9vqjf **ORCID:** https://orcid.org/0000-0002-4413-5527 Content not peer-reviewed by ChemRxiv. **License:** CC BY-NC-ND 4.0

(46) Taylor, N.; Ma, W. J.; Kristopeit, A.; Wang, S. C.; Zydney, A. L. Enhancing the performance of sterile filtration for viral vaccines and model nanoparticles using an appropriate prefilter. *Journal of Membrane Science* **2022**, *647*.

(47) Baron-Epel, O.; Gharyal, P. K.; Schindler, M. Pectins as mediators of wall porosity in soybean cells. *Planta* **1988**, *175*.

(48) Kornecki, M.; Mestmäcker, F.; Zobel-Roos, S.; Figueiredo, L. H. D.; Schlüter, H.; Strube, J. Host cell proteins in biologics manufacturing: The good, the bad, and the ugly. *Antibodies* **2017**, *6*.

(49) Travers, P.; Walport, M.; Shlomchik, M.; Janeway, C. *The structure of a typical antibody molecule - Immunobiology - NCBI Bookshelf*; 2001.

https://doi.org/10.26434/chemrxiv-2024-9vqjf **ORCID:** https://orcid.org/0000-0002-4413-5527 Content not peer-reviewed by ChemRxiv. **License:** CC BY-NC-ND 4.0